[34]G. Busch, P. Cotti, and P. Munz, Solid State Commun. 7, 795 (1969).

[35]D. E. Eastman, F. Holzberg, and S. Methfessel, Phys. Rev. Letters 23, 226 (1969).

[36]S. T. Manson and J. W. Cooper, Phys. Rev. 165, 126 (1968).

[37]P. Jaegle and G. Missoni, Compt. Rend. 71, 262 (1966).

[38]A. H. Wilson, The Theory of Metals (Cambridge U. P., New York, 1936), p. 133.

[39]A. I. Golovashkin, A. I. Kopeliovich, and G. P. Motulevich, Zh. Eksperim. i Teor. Fiz. 53, 2053 (1967) [Soviet Phys. JETP 26, 1161 (1968)]; W. A. Harrison, Phys. Rev. 147, 467 (1966).

[40]A. O. E. Animalu and V. Heine, Pseudopotentials in the Theory of Metals, edited by W. A. Harrison (Benjamin, New York, 1966), p. 309.

[41]C. Moore, Atomic Energy Levels, Natl. Bur. Std. (U. S.) Circ. No. 467 (U. S. GPO, Washington, D. C., 1949), Vols. 2 and 3.

[42]O. K. Andersen and T. L. Loucks, Phys. Rev. 167, 551 (1968).

[43]C. N. Berglund and W. E. Spicer, Phys. Rev. 136, A1030 (1964); 136, A 1044 (1964).

[44]N. V. Smith, in Proceedings of the Density of States Conference, Natl. Bur. Std., Washington, D. C., 1969 (unpublished).

[45]W. E. Spicer, Ref. 44.

Size Effects and Doppler-Shifted Cyclotron Resonance of Helicons in Copper[†][*]

L. T. Wood[‡] and J. D. Gavenda

Department of Physics, University of Texas, Austin, Texas 78712

(Received 9 January 1970)

Gantmakher-Kaner (GK) oscillations and Doppler-shifted cyclotron resonance (DSCR) of helicons have been investigated in very pure copper with the magnetic field $\vec{B}_0$ and the propagation vector $\vec{q}$ along the [101], [001], and [111] directions. The results are compared with a model Fermi surface proposed by Halse. For $\vec{B}_0 \parallel [101]$, the GK mode is excited by a heavily damped helicon which enhances the effective skin depth for certain values of q. Using a period of 314 ± 7 G for the GK oscillations, we assign a value of $|m_c \bar{v}_z|_{ext} = (0.648 \pm 0.014)$ $\times 10^{-19}$ g cm sec^{-1} to electrons with orbits near the plane $a |k_z| = 2.675$, where a is the lattice constant, m_c the cyclotron effective mass, and $\bar{v}_z$ the drift velocity along $\vec{B}_0$. The value of $|m_c \bar{v}_z|_{ext}$ calculated from the model Fermi surface is 0.609×10^{-19} g cm sec^{-1}. Damping of the helicon by open-orbit electrons near the planes $a |k_z| = 4.225 - 4.625$ has also been observed. For $\vec{B}_0 \parallel [001]$, no GK oscillations were observed; we attribute this to the large-amplitude oscillations in v_z for electron orbits near the plane $a |k_z| = 1.95$. The helicon edge does not appear to be a measure of $|m_c \bar{v}_z|_{max}$ since $|m_c \bar{v}_z|$ may go to infinity around the necks. For $\vec{B}_0 \parallel [111]$, GK oscillations with a period of 590 ± 7G were observed. This period yields $|m_c \bar{v}_z|_{ext} = (1.26 \pm 0.02) \times 10^{-19}$ g cm sec^{-1} for electron orbits near the plane $a |k_z| = 3.625$, while the value calculated from the model Fermi surface is 1.34×10^{-19} g cm sec^{-1}. We emphasize that alignment of $\vec{B}_0$ along a crystal axis can be extremely critical, particularly when open-orbit electrons are present.

I. INTRODUCTION

It is well known that electromagnetic waves are generally strongly damped in metals. If, however, one applies a sufficiently strong magnetic field to a pure metal at low temperatures, circularly polarized electromagnetic waves known as helicons can propagate through the metal. The criterion for such waves to propagate is $\omega_c \tau \gg 1$, where ω_c and τ are the conduction-electron cyclotron frequency and relaxation time, respectively. Physically, this means that the electrons are able to complete many cyclotron orbits before they undergo scattering.

Helicons were predicted in 1960 by Aigrain[1] and by Konstantinov and Perel[2] and observed in 1961 by Bowers, Legendy, and Rose.[3] The early helicon experiments[3-7] were directed at determining the Hall coefficients of metals. A proposal by Stern,[8] however, brought to light the fact that helicons could be used to obtain information about the Fermi surface. Stern proposed that helicons could undergo Doppler-shifted cyclotron resonance (DSCR) in much the same way that circularly polarized sound waves undergo DSCR.[9] Suppose a helicon of angular frequency ω and wave number q is propagating in a metal. Let the propagation vector $\vec{q}$ and the applied magnetic field $\vec{B}_0$ both lie along the z axis. An electron with an average velocity $\bar{v}_z$ in the direction of the applied field experiences a Doppler-shifted frequency ω_e given by

$$\omega_e = \omega + q \bar{v}_z \ . \tag{1}$$

If ω_e coincides with ω_c, the electrons can absorb energy from the helicon. For magnetic field values such that $\omega_c < \omega_e^{max}$, where $\omega_e^{max} = \omega + q\bar{v}_z^{max}$, there will be some electrons which have the proper $\bar{v}_z$ so that $\omega_c = \omega_e$. These electrons absorb energy from the helicon so that it will not propagate. However, for fields such that $\omega_c > \omega_e^{max}$, there will no longer be any electrons capable of matching the effective frequency of the helicon even when $\bar{v}_z$ is a maximum, no energy will be absorbed via the DSCR mechanism, and the helicon will propagate. The condition $\omega_c = \omega_e^{max}$ defines the Kjeldaas edge or absorption edge. Under normal experimental conditions, $\omega \ll q\bar{v}_z^{max}$ so that the absorption edge condition can be written as

$$(m_c\bar{v}_z)_{max} = eB_E/cq_E \quad , \tag{2}$$

where B_E and q_E are the values of B_0 and q measured at the absorption edge. Among those metals whose Fermi surfaces have been studied using DSCR of helicons are polycrystalline sodium, potassium, and indium, [10] and single-crystal aluminum. [11]

To date a great deal of the theoretical work concerning helicons has been based on the assumption that the wave propagates in an infinite medium. The infinite-medium dispersion relation has been used quite effectively to analyze helicon propagation in a thin metal slab provided the thickness of the slab is much less than the other two dimensions and provided the electrons undergo specular reflection at the boundaries. The infinite-medium dispersion relation is given by

$$q_\pm^2 = (4\pi\omega/ic^2)\sigma_\pm \quad , \tag{3}$$

where $\sigma_\pm$ is the conductivity for the left and right circularly polarized waves. If, however, one includes the effects of the boundaries and calculates the ratio of the transmitted electric field to the incident electric field, the size-effect oscillations predicted by Gantmakher and Kaner[12] can be observed. These oscillations are interpreted as coming from electrons with an extremal value of $m_c\bar{v}_z$. A large group of electrons having the same $(m_c\bar{v}_z)_{ext}$ can generate a substantial field at the specimen surface provided they complete an integral number of revolutions while traversing the specimen. The period of the Gantmakher-Kaner (GK) oscillations can be related to the Fermi-surface topology. In particular,

$$(m_c\bar{v}_z)_{ext} = (eL/2\pi c)\Delta B_0 \quad , \tag{4}$$

where L is the specimen thickness and ΔB_0 is the period of the oscillations measured in units of the magnetic field.

The purpose of this paper is to present detailed results of GK size-effect measurements and to investigate DSCR of helicons in single-crystal copper along the [001], [110], and [111] directions. These results are then related to the Fermi surface of copper. Finally, it is shown that information similar to that obtained by magnetoresistance measurements can also be obtained from helicon experiments.

In Sec. II, the theoretical ideas are presented. In Sec. III, the experimental techniques are described in detail, and in Sec. IV, the results and their interpretation are presented for each of the three highest-symmetry directions.

II. THEORY

The general dispersion relation for a plane electromagnetic wave in an infinite nonmagnetic medium of dielectric constant K is

$$\det(\underline{\sigma} - \underline{M}) = 0 \quad , \tag{5}$$

where $\underline{\sigma}$ is the conductivity tensor of the medium and

$$\underline{M} = (ic^2/4\pi\omega)[q^2\underline{1} - \vec{q}\vec{q} - (\omega^2/c^2)K\underline{1}] \quad . \tag{6}$$

For frequencies used in the experiment, the displacement current can be neglected so that one obtains

$$\underline{M} = (ic^2/4\pi\omega)(q^2\underline{1} - \vec{q}\vec{q}) \quad . \tag{7}$$

If a static magnetic field $\vec{B}_0$ and the propagation vector $\vec{q}$ of the electromagnetic wave both lie along the z axis, and if there is at least twofold symmetry about this axis, then the conductivity can be written as

$$\underline{\sigma} = \begin{pmatrix} \sigma_{xx} & \sigma_{xy} & 0 \\ -\sigma_{xy} & \sigma_{yy} & 0 \\ 0 & 0 & \sigma_{zz} \end{pmatrix} \quad , \tag{8}$$

where each component of $\underline{\sigma}$ may depend on the frequency ω, the wave number q, and the applied magnetic field B_0. If Eq. (8) is substituted into Eq. (5), one obtains

$$q_\pm^2 = -\frac{4\pi i\omega}{c^2}\left[\frac{(\sigma_{xx}+\sigma_{yy})}{2} \mp \sigma_{xy}\left(-1+\frac{(\sigma_{xx}-\sigma_{yy})^2}{4\sigma_{xy}^2}\right)^{1/2}\right] \tag{9}$$

for the dispersion relation. The ratio of the y component of the electric field to the x component is given by

$$\frac{E_y}{E_x} = \frac{(\sigma_{yy}-\sigma_{xx})}{2\sigma_{xy}} \mp \left(-1+\frac{(\sigma_{yy}-\sigma_{xx})^2}{4\sigma_{xy}^2}\right)^{1/2} \quad . \tag{10}$$

Equations (9) and (10) describe an elliptically polarized plane wave traveling in the z direction when, for an uncompensated metal, the magnetic field is large enough so that $\sigma_{xy} \gg \sigma_{xx}$ and $\sigma_{xy} \gg \sigma_{yy}$. Under these conditions $\text{Re}q \gg \text{Im}q$, and the wave

$$(n\pi/L)^2 = -(4\pi i\omega/c^2)\sigma_+(n\pi/L) \ . \tag{24}$$

If the conductivity is local, one obtains

$$n = 2L(\omega n_e e/\pi c)^{1/2} B_0^{-1/2} \ . \tag{25}$$

The branch points of the conductivity are caused by electrons at an extremum in $m_c \bar{v}_z$. Each branch point contributes an oscillatory term, and since the numerator of Eq. (22) alternates in sign, the period of the electric field is related to $|m_c \bar{v}_z|_{ext}$ by

$$\left| m_c \bar{v}_z \right|_{ext} = (eL/2\pi c)\Delta B_0 \ . \tag{26}$$

III. EXPERIMENTAL TECHNIQUES

A. Transmission Method

The technique employed in studying the transmission of helicons is similar to that used by Grimes and Buchsbaum.[19] Signals are coupled into the copper specimen by means of a small coil of rectangular cross section having about 200 turns of No. 42 wire placed as close to the specimen as possible. A similar coil on the other side of the specimen picks up the transmitted signal. Generally, the axes of the two coils are perpendicular to minimize the signal which couples directly from one coil into the other.

A block diagram of the experimental apparatus is shown in Fig. 1. At zero magnetic field the externally coupled signal is cancelled by adding to it a signal of the proper phase and amplitude. The phase of this signal is controlled by the variable delay line. As the magnetic field is increased and an absorption edge is passed, the helicon begins to propagate. The helicon signal (whose strength may be on the order of 50 μV when the voltage across the input coil is about 3 V) goes into a wide-band amplifier with a gain of about 54 dB. It then passes through a phase shifter and finally into one input of a double-balanced mixer. A reference signal from the oscillator is fed into the second input of the mixer. The output from the mixer consists of the sum and difference frequencies of the two input signals. For input signals of the same frequency, the difference signal is just dc. By using an appropriate low-pass filter, the high-frequency component of the signal can be filtered leaving only the dc signal. The amplitude of this dc signal is proportional to the cosine of the phase angle between the reference signal and the helicon signal, and to the amplitude of the helicon signal. This signal is then amplified or differentiated before being connected to one axis of an x-y recorder. The other axis of the recorder is driven by a signal from a rotating-coil gaussmeter.

To understand how this system allows us to detect the helicon signal, note first of all that the
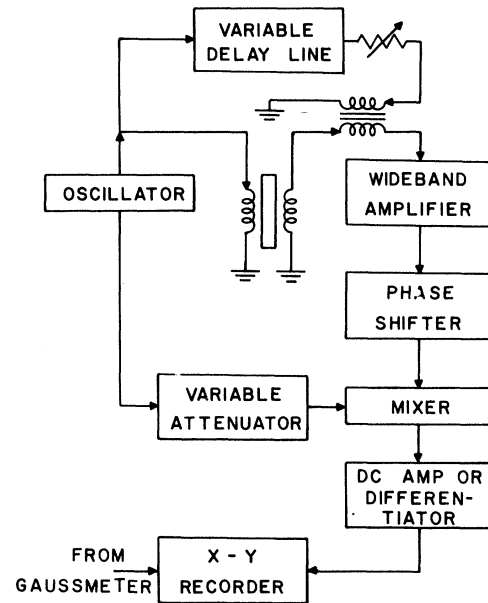
FIG. 1. Schematic of experimental apparatus.

helicon signal has both an amplitude and a phase with respect to the reference signal. Both the amplitude and phase of the helicon depend on the strength of the magnetic field B_0. In the local regime ($ql \ll 1$, a condition satisfied for magnetic fields reasonably far above the absorption edge), the wave-number dependence of the helicon on the field B_0 and the frequency ω is given by Eq. (17). For a given frequency the wavelength of the helicon increases as the square root of the field. As the field is increased the number of helicon half-wavelengths in a specimen of a given thickness L decreases. This means that, as the number of helicon half-wavelengths in the specimen changes from N to $N-1$ (this is the case for increasing field), the phase of the helicon signal with respect to the reference signal changes by π. Therefore, the recorder output changes from a maximum to a minimum or vice versa.

B. Specimen Preparation

The manner of preparing the copper specimens used in these experiments is very important. The specimens were all cut from a boule[20] having a resistivity ratio of 35 000 as measured by the eddy-current-decay method. The specimens were first cut into rectangular slabs about 8×8×1 mm. They were x rayed using a standard Laue back reflection technique and then spark-planed. The crystal axis was within 0.3° of perpendicular to the specimen face in all specimens.

After each specimen had been planed, its thick-

ness was carefully measured with a micrometer. If the specimen did not have the same thickness on each corner to within 0.0001 in., it was x rayed and spark-planed again.

This accuracy was necessary in preparing the specimens because, if reasonably large helicon signals or GK oscillations were to be seen, the faces of a specimen had to be flat and parallel to within a fraction of a helicon half-wavelength. For a frequency of 200 kHz and a field of 20 kG, the wavelength of a helicon propagating along the [001] axis in copper is about 7×10^{-3} cm. This means that the specimen faces had to be flat and parallel to within much better than 0.003 in.

When the specimen was found acceptable, it was etched very lightly in dilute nitric acid to remove surface damage. Care was taken to see that the etching was done evenly. The specimen was then x rayed once again to insure that the crystal axis was still normal to the specimen face.

C. Specimen Holder

The form of construction of the specimen holder was very important in carrying out these experiments. First of all, the specimen holder had to be constructed so that the transmitting and receiving coils were extremely close to the specimen. In the usual experiment, the coils were within one- or two-thousandths of an inch of the specimen. The following steps were taken to insure

FIG. 3. Schematic showing how the specimen is tilted in the liquid helium.

FIG. 2. Schematic showing how the specimen is mounted between the transmitting and receiving coils.

good coupling of the signals into the specimen. A square hole whose dimensions were slightly greater than the specimen dimensions was cut into a plate which matched the thickness of the specimen. The coils (about 200 turns of No. 42 copper wire) were wound on phenolic coil forms about $\frac{3}{16}$ in. square and about $\frac{1}{10}$ in. thick. These coil forms were fitted into holes in two other brass plates so that the coil surfaces were even with the faces of the plate. Silver paint was placed around the specimen to help shield the coils from one another and the three plates were fastened together with screws. Figure 2 shows this arrangement. By exercising reasonable care, one can achieve good coupling of signals into and out of the specimen.

The plates containing the mounted specimen were fitted into a box which allows the specimen to be tilted in the vertical plane. The tilting was accomplished by a micrometer located at the top of the holder and connected to the spring-loaded lever arm of the box. This arrangement is shown in Fig. 3. A 0.0005-in. linear movement of the micrometer corresponds to 4' of arc and the system is linear for small angles of tilt.

D. Specimen Alignment in Magnetic Field

The presence of open-orbit electrons with the magnetic field in certain directions can cause the

FIG. 4. Transmitted signal versus tilt angle between $\vec{B}_0$ and [101]. The tilt is about [10$\bar{1}$] with $B_0 = 23.1$ kG, $f = 200$ kHz, and rotation angle $= -0.2°$.

amplitude of the detected signal to vary drastically as a function of the magnetic field direction. Therefore, some caution must be exercised when aligning the crystal axis along the magnetic field. T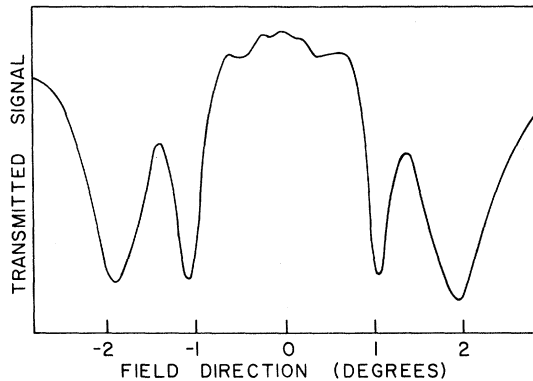he magnetic field is first set to a high value and the crystal is oriented so that the crystal axis is approximately parallel to the magnetic field. The detected signal is plotted as a function of the tilt angle as the tilt angle is swept through about 7° in intervals of 4' while the field rotation angle is kept constant. A symmetry line is then located in the plot. The tilt angle is set at the symmetry value and the field rotation angle is swept through about 7° in 0.1° intervals. The symmetry line is then located for this plot. The angles obtained from the two symmetry lines should determine the crystal axis. Figures 4 and 5 show representative plots of the signal strength versus tilt angle for a fixed rotation angle and the signal strength versus rotation angle for a fixed tilt angle.

The technique described above works provided there is twofold or fourfold symmetry about the axis in question and provided that the specimen is cut and mounted in such a way that one crystal axis is parallel to either the tilt or rotation axis. If the latter criterion is not met, the following steps are taken to align the magnetic field along the crystal axis. The magnetic field is again set to a high value and the crystal is oriented so that the crystal axis is approximately parallel to the magnetic field. The detected signal is plotted as a function of tilt angle while the field rotation angle is kept constant. In general, there will be no symmetry line in this plot. The field rotation angle is changed to a new value and the detected signal is plotted as the tilt angle is varied. This process is repeated until one of the plots shows a symmetry line. The angles for which the symmetry lines oc-

cur determine the crystal axis. To check these angles the tilt angle is set to that value determined by the symmetry line and the detected signal is plotted as a function of the field-rotation angle. There should be a symmetry line in this plot if the crystal axis has been correctly determined.

IV. EXPERIMENTAL RESULTS AND INTERPRETATION

A. Results and Interpretation for $\vec{B}_0 \parallel [101]$

In Figs. 6–8, we show representative curves with $\vec{B}_0$ along or near [101]. Some general comments concerning the curves may be helpful. First of all, the labeling of the ordinate as the transmitted signal is a convenient notation. One should remember that this signal is really the result of beating a reference signal with the signal picked up by the receiving coil. Second, in order to enhance rapidly varying signals while suppressing slowly varying signals, a differentiator was employed in some of the experiments. The differentiator enhances the GK oscillations without enhancing the more slowly varying background changes in the signal. The differentiation is actually with respect to time, but, since the magnetic field sweep is linear in time, it is equivalent to differentiation with respect to the field. In Fig. 6, we show the transmitted signal versus B_0 with $\vec{B}_0$ along [101] while in Fig. 7 we show the differentiated transmitted signal versus B_0 with $\vec{B}_0$ along [101]. In Fig. 8, we show the transmitted signal versus B_0 for $\vec{B}_0$ tilted 2.0° away from [101] toward [010]. Figures 6 and 7 show the GK oscillations (the closely spaced oscillations), but only Fig. 8 shows any sizable helicons. We will come to the explanation of this important dif-
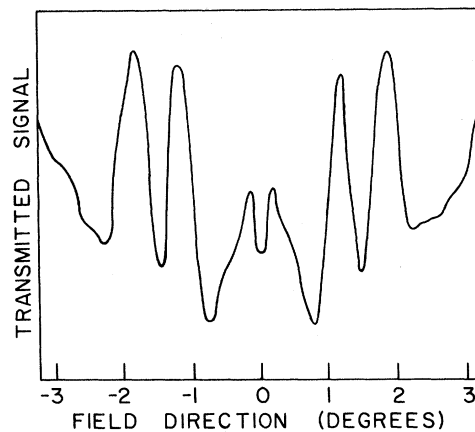

FIG. 5. Transmitted signal versus rotation angle between $\vec{B}_0$ and [101]. The rotation is about [010] with $B_0 = 23.1$ kG, $f = 200.0$ kHz, and tilt angle $= -2.0°$.
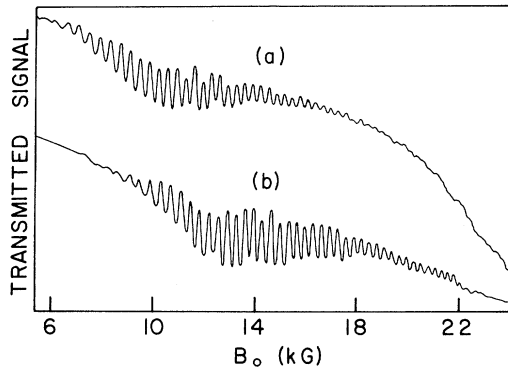
FIG. 6. Transmitted signal versus B_0 for $\vec{B}_0 \parallel [101]$ with $f = 250.0$ kHz in (a) and $f = 530.8$ kHz in (b). The specimen thickness is 0.81 mm and $T = 4.2$ °K for all experimental curves with $\vec{B}_0$ along or near [101].
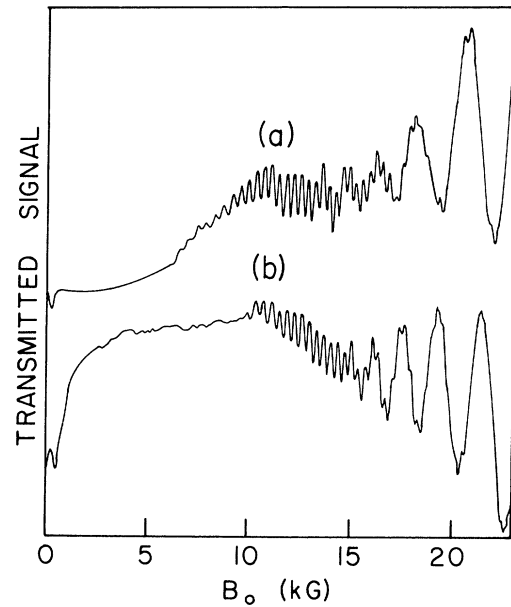

FIG. 8. Transmitted signal versus B_0 for $\vec{B}_0$ tilted 2.0° away from [101] toward [010] with $f = 321.6$ kHz in (a) and $f = 445.4$ kHz in (b).

ference shortly, but we now wish to consider the GK oscillations in detail.

Recall from Sec. II that the mathematical origin of the GK oscillations lies in the branch points of the conductivity. Physically, they may arise when a large number of electrons with the same $|m_c \bar{v}_z|$ arrive in phase at the surface of the specimen. The period of the GK oscillations is related to either a maximum or an extremum in $|m_c \bar{v}_z|$, denoted by $|m_c \bar{v}_z|_{max}$ and $|m_c \bar{v}_z|_{ext}$, respectively. However, the existence of a maximum or an extremum does not necessarily mean that GK oscillations will have a large enough amplitude to be seen experimentally. One must consider the details of the Fermi surface in order to predict the amplitude of the GK oscillations.

Antoniewicz[21] has pointed out that, for a Fermi surface which has an extremum in $|m_c \bar{v}_z|$ as a function of k_z as well as $|m_c \bar{v}_z| > |m_c \bar{v}_z|_{ext}$, it is possible for a helicon to propagate at fields lower

than the usual absorption edge. This he called the helicon "window." Figure 9 shows a plot of $|m_c \bar{v}_z|$ versus $|k_z|$ for a model Fermi surface[22] which has the features necessary to show a heli-
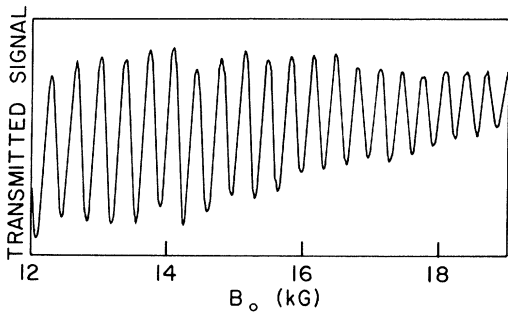

FIG. 7. Transmitted signal versus B_0 for $\vec{B}_0 \parallel [101]$ with $f = 550.0$ kHz.
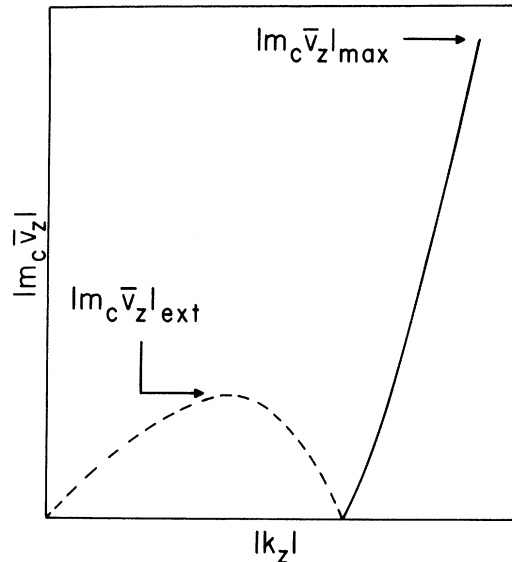

FIG. 9. $|m_c \bar{v}_z|$ versus $|k_z|$ for Fermi surface proposed by Eckstein. The dashed line indicates where $m_c \bar{v}_z$ is positive.
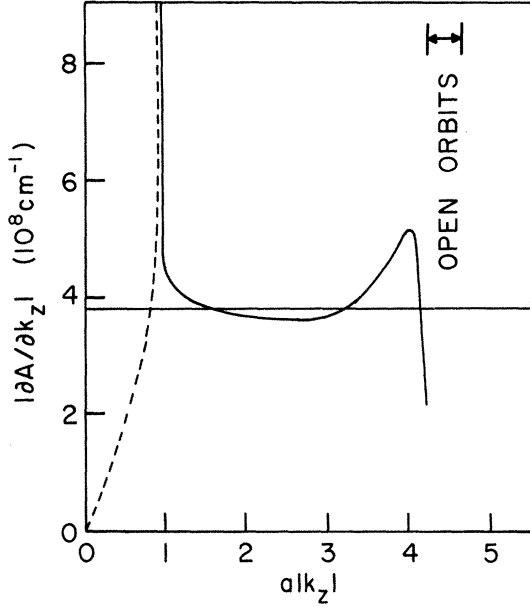
FIG. 10. $|\partial A/\partial k_z|$ versus $a\,|k_z|$ for the Fermi surface of copper with k_z along [101]. a is the lattice constant. The dashed line indicates where $\partial A/\partial k_z$ is positive, the solid where it is negative. The horizontal line represents the experimental value of $|\partial A/\partial k_z|_{\rm ext}$.

surface of copper. The period of the GK oscillations should be related to the value of $|\partial A/\partial k_z|_{\rm ext}$ shown in Figs. 10 and 11 since there are a large number of electrons with $|m_c \bar{v}_z|_{\rm ext}$.

To understand what happens in the cases where the curves show no helicon but do show GK oscillations, we refer to Fig. 10. The periodic open-orbit electrons from $a\,|k_z| = 4.225$ to $a\,|k_z| = 4.625$ severely damp the helicon.[26, 27] Physically, this damping arises from the fact that these open-orbit electrons can carry current in only a single direction. Therefore, this current cannot possibly remain perpendicular to the rotating electric field of the helicon. This means that the Joule heating can become quite large, energy is dissipated, and the helicon does not propagate. However, these open-orbit electrons have the same damping effect as electrons for which $|m_c \bar{v}_z| > |m_c \bar{v}_z|_{\rm ext}$. The condition for the helicon window is satisfied and the window shows up as GK oscillations when the boundary conditions are imposed.

We can explain qualitatively the structure of the polar plot in Fig. 4 by considering the shape of the portion of the Fermi surface responsible for the open orbits. Figure 12 shows the band of open-orbit electrons when $\vec{B}_0 \parallel [101]$. In principle, as soon as $\vec{B}_0$ is tilted the slightest bit off axis these

con window. Those electrons with $|m_c \bar{v}_z|_{\rm max}$ give rise to the usual absorption edge so that the helicon is highly damped below this absorption edge. For those electrons with $|m_c \bar{v}_z|_{\rm ext}$, the damped helicon enhances the effective skin depth for certain values of q; that is, it appears as though the electric field has penetrated throughout the sample. The electrons with $|m_c \bar{v}_z|_{\rm ext}$ can gain energy from this damped helicon provided the mismatch between the helical wavelength of the GK mode and a Fourier component of the helicon mode is not too great.[23] At high fields the mismatch of the wavelengths causes the GK oscillations to die out as the curves show. At the low fields the damping of the helicon is so great that the enhancement of the skin depth is not a significant factor.

The data are analyzed by making use of a relation derived by Harrison,[24] namely,

$$ m_c \bar{v}_z = -\left(\frac{\hbar}{2\pi}\right)\left(\frac{\partial A}{\partial k_z}\right)_{\epsilon_F} \tag{27} $$

Figures 10 and 11 show $|\partial A/\partial k_z|$ versus $a\,|k_z|$ for the Fermi surface of copper with $\vec{B}_0 \parallel [101]$ and for $\vec{B}_0$ tilted $2°$ away from [101] toward [010], respectively. Here a is the lattice constant. The values of $|\partial A/\partial k_z|$ shown in these curves were calculated using Halse's[25] constants for the Fermi

FIG. 11. $|\partial A/\partial k_z|$ versus $a\,|k_z|$ for the Fermi surface of copper with k_z tilted $2.0°$ away from [101]. The solid horizontal line represents the experimental value of $|\partial A/\partial k_z|_{\rm max}$. The dashed horizontal line represents the experimental value of $|\partial A/\partial k_z|_{\rm ext}$. $\partial A/\partial k_z$ is negative where the line is solid and positive where the line is dashed.
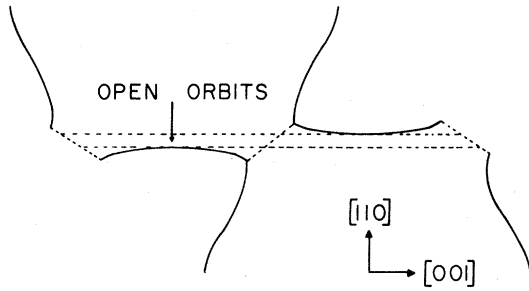
FIG. 12. Central section of the copper Fermi surface in the (110) plane. The open-orbit electrons are those having k_z values between the two dashed parallel lines.

open orbits become long extended closed orbits. Because of finite mean free path, however, the electrons may be scattered before completing this extended orbit and thus will have the effect of an open orbit. The drastic change in signal in Fig. 4 as we move from $0.7°$ to $1.0°$ off axis is the result of the open orbits changing into extended closed orbits.

We now wish to consider what information can be obtained from the GK oscillations. We have already seen that the period of the GK oscillations should be related to electrons with $|m_c \bar{v}_z|_{ext}$. However, a close investigation reveals that the GK oscillations are not strictly periodic. The oscillations at the low fields have a period of about 400 G, while the oscillations at the high fields have a period of about 310 G. In relating the GK oscillations to the Fermi surface, we must decide whether to choose the low-field period, the high-field period, or some average period.

In order to determine which period to use, Antoniewicz[28] has evaluated the conductivity for a rather special Fermi surface on which m_c and v_z are constants, in the limit as $\omega_c \tau \to \infty$. Using these assumptions the conductivity can be evaluated in closed form. Equation (11) can then be used to get an explicit form for the dispersion relation, in particular,

$$q^2 = \frac{\omega_c \pm [\omega_c^4 - 16\pi\omega\omega_c\sigma_0\bar{v}_z^2/c^2\tau]^{1/2}}{2\bar{v}_z^2} \quad . \qquad (28)$$

This dispersion relation has two branches which, in the limit of large B_0, become

$$q^2 = \omega_c^2/\bar{v}_z^2 \qquad (29)$$

and

$$q^2 = 4\pi\omega n_e e/cB_0 \quad . \qquad (30)$$

Equation (29) is just the dispersion relation for the GK mode and Eq. (30) is the dispersion relation for the helicon mode in the local regime.

Since the dispersion relation yields a pure-GK mode and a pure-helicon mode only at high fields, then the high-field oscillations correspond to the pure-GK mode and they should be used in relating the GK periods to the Fermi surface. At the intermediate fields the helicon mode and the GK mode are mixed and it is this mixing which gives rise to the monotonic change in the period of the GK oscillations with field.

In most of the curves the last seven or eight oscillations are reasonably periodic so we will use the average period of the last seven oscillations to determine the experimental value of $|m_c \bar{v}_z|_{ext}$. This average period is 314 ± 7 G. This means that $|m_c \bar{v}_z|_{ext} = (0.648 \pm 0.014) \times 10^{-19}$ g cm sec^{-1} or $|\partial A/\partial k_z|_{ext} = (3.86 \pm 0.08) \times 10^8$ cm^{-1}. The horizontal line in Fig. 10 represents the experimental value of $|\partial A/\partial k_z|_{ext}$. The value of $|\partial A/\partial k_z|_{ext}$ from Halse's Fermi surface in Fig. 10 is 3.65×10^8 cm^{-1} so the values are within 6% of each other. It should also be pointed out that the period of the GK oscillations changes by less than 1% as the field is tilted $2°$ off axis. This also agrees with the result one expects from the calculated value of $|\partial A/\partial k_z|_{ext}$ when $\vec{B}_0$ is tilted off axis by $2°$ (see Fig. 11).

We will now consider the information that can be obtained by investigating the helicon oscillations. For simplicity we assume that an extremum in the signal occurs when there is an integral number of helicon half-wavelengths in the specimen. This may not be strictly true because of phase changes which can occur at the boundary. The number of half-wavelengths in the specimen is given by Eq. (25). If both electrons and holes are present, Eq. (25) can be written as

$$n = 2L(\omega n_{eff} e/\pi c)^{1/2} B_0^{-1/2} \quad , \qquad (31)$$

where $n_{eff} = n_e - n_h$. To determine the number of half-wavelengths we assume that an extremum in the signal occurs when there are n_1 half-wavelengths in the specimen. The next extremum in the signal occurs when there are $n_1 - 1$ half-wavelengths in the specimen (this is the case if the second extremum occurs at a higher field than the first). We then plot n versus $B_0^{-1/2}$. From Eq. (31) it can be seen that when $B_0^{-1/2} = 0$, one obtains $n = 0$. The curve is adjusted to pass through the origin and one reads n directly from the graph. Figure 13 shows such a plot. At high fields (small $B_0^{-1/2}$) the points lie on a straight line indicating that the local dispersion relation is satisfied. At low fields q is large enough that $ql > 1$ and there is a deviation from the local dispersion relation as the nonlocal regime is entered. Recall that $q = n\pi/L$ so we can consider graphs of n versus $B_0^{-1/2}$ to be equivalent to graphs of q versus
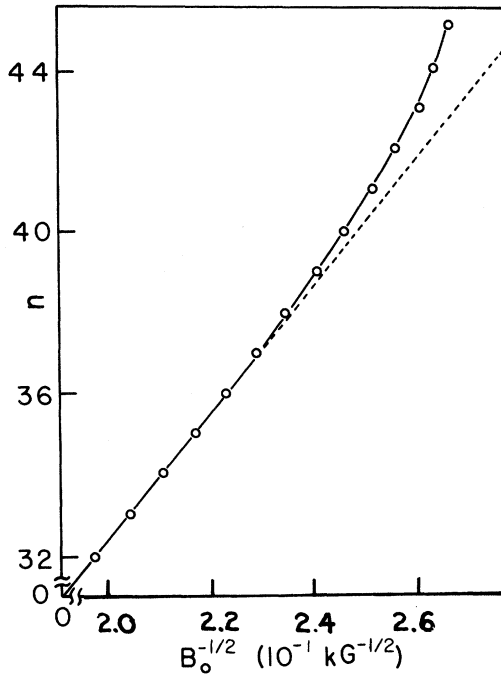
FIG. 13. Number of helicon half-wavelengths in the specimen versus $B_0^{-1/2}$. The dashed line shows the behavior if the local dispersion relation were valid near the edge. $\vec{B}_0$ tilted 2° away from [101], $f=445.37$ kHz.

$B_0^{-1/2}$. From the slope of the straight line in Fig. 13 one can determine the number of effective electrons n_{eff} by using Eq. (31). The average value of n_{eff} is 6.9×10^{22} cm^{-3}. This compares with a free-electron value of 8.4×10^{22} cm^{-3} and a value of 5.3×10^{22} cm^{-3} determined from magnetoresistance measurements.[29] The value of n_{eff} obtained from Halse's surface is 4.7×10^{22} cm^{-3}. The reason for the discrepancy in the experimental and calculated values of n_{eff} is that the local regime may not have been reached even for the largest values of B_0. If the curve shown in Fig. 13 still has a slight deviation from a straight line at high fields, then the slope of the straight line shown is too large thus giving a value of n_{eff} which is too large. A second reason for the discrepancy is that the calculated value of n_{eff} is for $\vec{B}_0 \parallel [101]$ while the experimental value is obtained for $\vec{B}_0$ tilted 2° away from the [101] axis. In the calculated value the open orbits are neglected. We can also determine $|m_c \bar{v}_z|$ for these electrons which cause the absorption edge. B_E is directly measured in the experiment and n at B_E can be determined from Fig. 13. Since $q = n\pi/L$, q_E can be calculated and $|m_c \bar{v}_z|_{max}$ can be calculated from Eq. (19). The value of $|m_c \bar{v}_z|_{max}$ is 1.3 $\times 10^{-19}$ g cm sec^{-1}. This gives a value of 7.6

$\times 10^8$ cm^{-1} for $|\partial A/\partial k_z|_{max}$. The calculated value of $|\partial A/\partial k_z|_{max}$ shown in Fig. 11 is 8.4×10^8 cm^{-1}. It has been pointed out[11,14] that there is not necessarily a correspondence between $|\partial A/\partial k_z|_{max}$ and that value of B_0 for which an infinity occurs in the slope of the curve obtained by plotting n versus $B_0^{-1/2}$. This lack of correspondence may explain the discrepancy between the experimental and calculated values of $|\partial A/\partial k_z|_{max}$.

It has also been shown[11] that for $\omega_c \tau \to \infty$ and for closed electron orbits $B_E \propto \nu^{1/3}$, where ν is the frequency. The graph in Fig. 14 shows the linear relationship between B_E and $\nu^{1/3}$. For a spherical Fermi surface the slope of this straight line is proportional to the Fermi radius, but for more complicated Fermi surfaces there may be no simple interpretation of the slope.

B. Results and Interpretation for $\vec{B}_0 \parallel [001]$

In Fig. 15 we show the transmitted signal versus B_0 for $\vec{B}_0 \parallel [001]$. For higher frequencies the absorption edge shifts to higher fields. The graph in Fig. 16 shows the linear relation between B_E and $\nu^{1/3}$.

The graph of n versus $B_0^{-1/2}$ (Fig. 17) shows the same behavior as Fig. 13 and the explanation for the shape of the graph is the same as given previously. From the slope of the straight line we calculate that $n_{eff} = 6.5 \times 10^{22}$ cm^{-3}. The value of
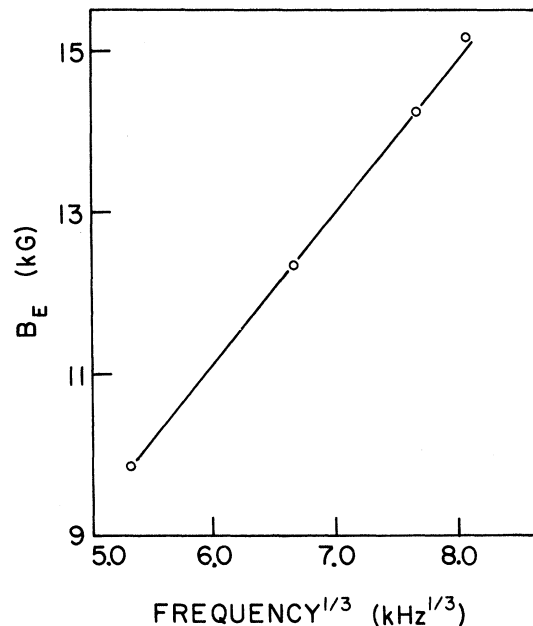

FIG. 14. The value of B_0 at the absorption edge versus the cube root of the frequency. B_0 tilted 2° away from [101].
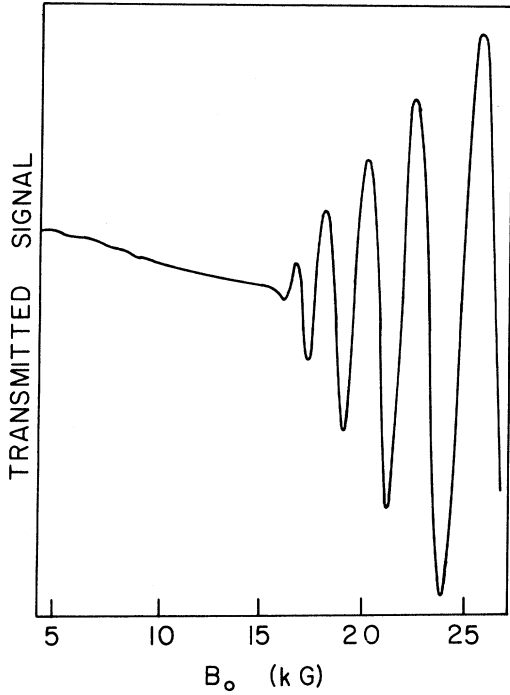
FIG. 15. Transmitted signal versus B_0 for $\vec{B}_0 \parallel [001]$ with $f = 395.3$ kHz. The specimen thickness is 0.84 mm and $T = 4.2\,°$K for all experimental curves with $\vec{B}_0$ along or near [001].
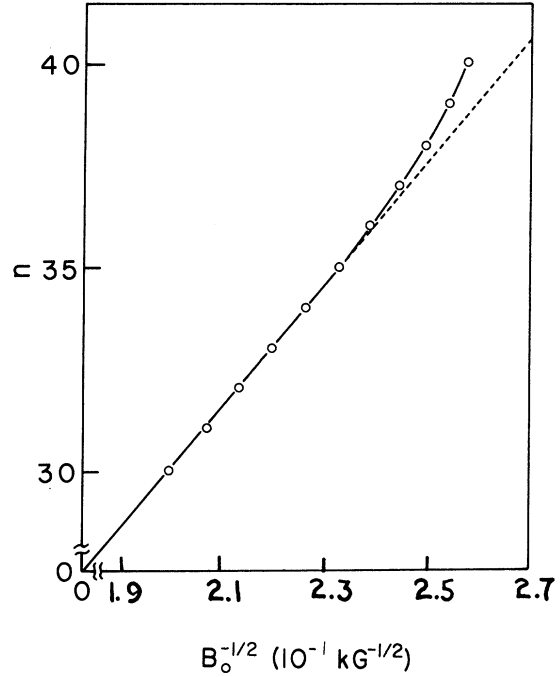

FIG. 17. The number of helicon half-wavelengths in the specimen versus $B_0^{-1/2}$. The dashed line shows the behavior if the local dispersion relation were valid near the edge. $\vec{B}_0 \parallel [001]$, $f = 395.26$ kHz.
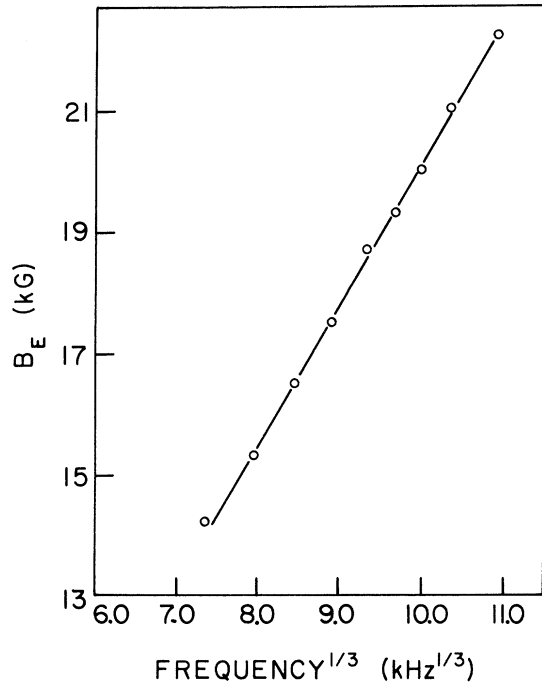

FIG. 16. The value of B_0 at the absorption edge versus the cube root of the frequency for $\vec{B}_0 \parallel [001]$.

n_{eff} from magnetoresistance data[29] is 4.3×10^{22} cm^{-3} and from Halse's Fermi surface $n_{eff} = 4.9 \times 10^{22}$ cm^{-3}. Once again the discrepancy in the experimental and calculated values of n_{eff} is probably due to the fact that the magnetic fields used were not large enough to get completely into the local regime.

In Fig. 18 we show the transmitted signal versus B_0 with the field tilted $+1.3°$, $0°$, and $-1.3°$ away from the [001] axis as determined from the polar plots in Fig. 19. The curves in Fig. 18 were all taken with the same gain setting so the reduction in amplitude of the helicon is a real effect. Once again this reduction in the amplitude of the signal is the result of damping by open-orbit electrons but the effects are not so pronounced as in the previous case. The same effect shows up in the magnetoresistance so that our data agree qualitatively with the magnetoresistance experiments.[29]

The value of $|m_c v_z|_{max}$ for those electrons responsible for the absorption edge is calculated in the same manner described in the previous section and is 1.6×10^{-19} g cm sec^{-1}. This value corresponds to $|\partial A/\partial k_z|_{max} = 9.5 \times 10^8$ cm^{-1}. In Fig. 20 we show $|\partial A/\partial k_z|$ versus $a|k_z|$ for $\vec{B}_0$
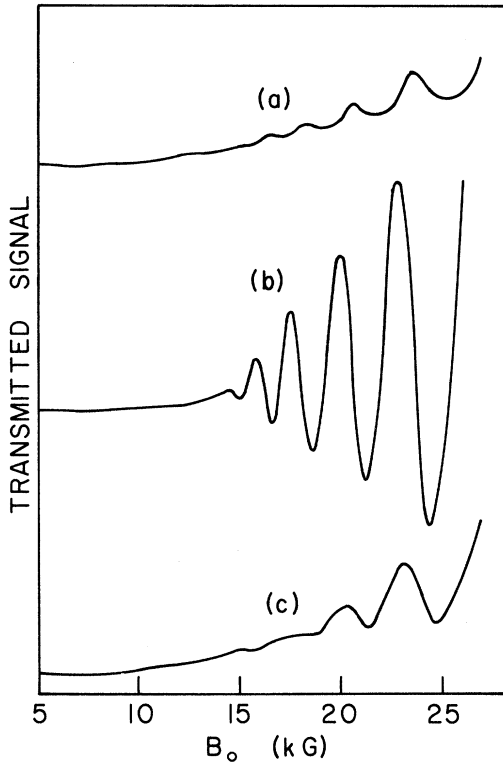
FIG. 18. Transmitted signal versus B_0 with $f = 300.0$ kHz. In (a) $\vec{B}_0$ is tilted 1.3° away from [001] toward [010] and in (c) $\vec{B}_0$ is tilted 1.3° away from [001] toward [0$\bar{1}$0]. In (b) $\vec{B}_0$ is along [001].

FIG. 20. $|\partial A/\partial k_z|$ versus $a|k_z|$ for copper Fermi surface with k_z along [001]. The horizontal line represents the experimental value of $|\partial A/\partial k_z|_{max}$. The dashed line indicates where $\partial A/\partial k_z$ is positive, the solid where it is negative.
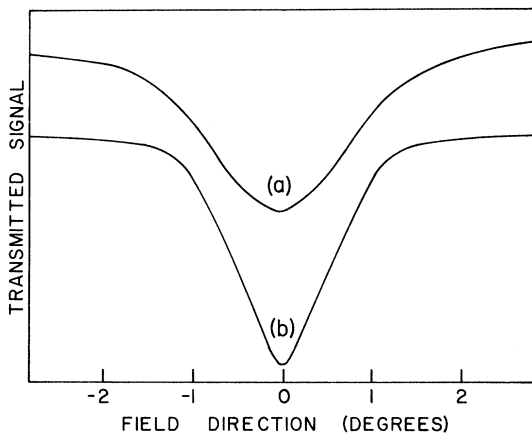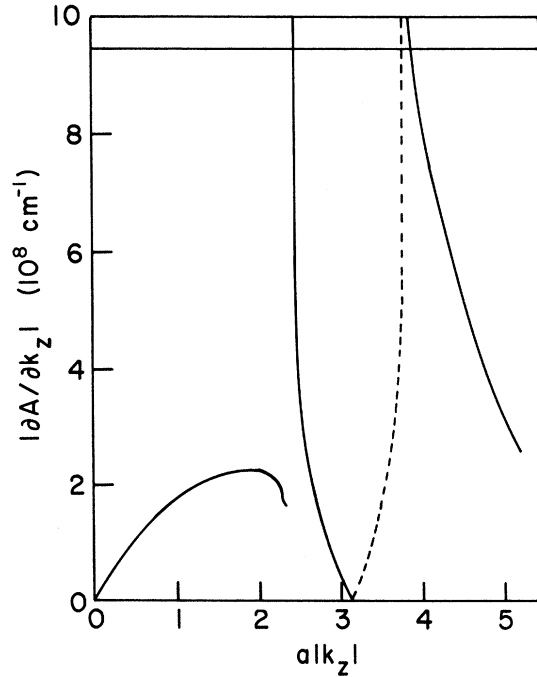
FIG. 19. (a) Transmitted signal versus rotation angle between $\vec{B}_0$ and [001]. The rotation is about [010] with $B_0 = 22.8$ kG, $f = 300.0$ kHz, and tilt angle $= 0.0°$. (b) Transmitted signal versus tilt angle between $\vec{B}_0$ and [001]. The tilt is about [100] with $B_0 = 22.8$ kG, $f = 300.0$ kHz, and rotation angle 0.0°.

along [001]. The experimental value of $|\partial A/\partial k_z|_{max}$ is indicated by the horizontal line. In this case the helicon edge does not seem to be a measure of $|\partial A/\partial k_z|_{max}$ since, in principle, $|\partial A/\partial k_z|$ may go to infinity on the plane that separates the electron and hole orbits.

One should also notice that there are no GK oscillations present in Fig. 15 even though the criteria to observe sizable GK oscillations are satisfied for this geometry. This is not to say that they do not exist, but we can say that their amplitude must be at least an order of magnitude smaller than in the [101] direction. A possible explanation for the absence of GK oscillations may be the large-amplitude oscillations in $\bar{v}_z$ for electrons with $|m_c\bar{v}_z|_{ext}$. In Fig. 21 we show v_z versus time for electrons at the plane $a|k_z| = 1.95$. Not only are there large-amplitude oscillations in v_z around this orbit, but these electrons actually have a negative value of v_z for a short time. This means that in real space they have a back and forth motion in the z direction. With this kind of motion it may not be possible for these electrons to remain in phase with the damped helicon in order to absorb energy from it. Under these circumstances the amplitude of the GK oscillations might be re-
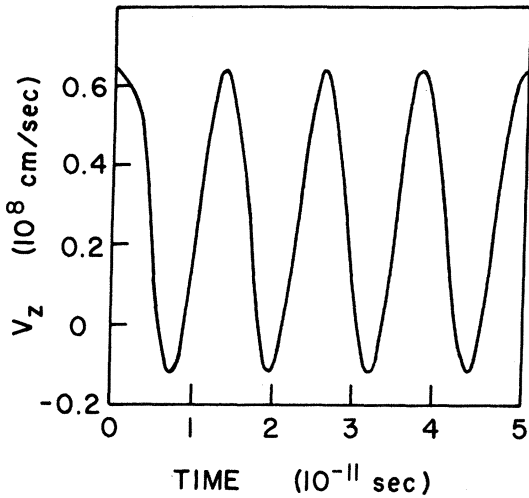
FIG. 21. The z component of velocity of an electron at $a\,|\,k_z\,| = 1.95$ versus time for $\vec{B}_0 \parallel [001]$ and $B_0 = 10$ kG.

duced considerably and would not be seen without increased sensitivity.

For comparison Fig. 22 shows v_z versus time for those electrons with $|m_c \bar{v}_z|_{ext}$ when $\vec{B}_0$ is parallel to the $[101]$ axis. The oscillatory behavior of v_z is not nearly so pronounced as with $\vec{B}_0 \parallel [001]$. This oscillatory behavior of v_z is a feature which a cylindrically symmetric Fermi surface does not show and, as is pointed out above, is not as prevalent with $\vec{B}_0 \parallel [101]$ where large-amplitude GK oscillations are present. We conclude then that, in order to determine whether sizable GK oscillations are to be observed in any given situation, it may be necessary to consider the behavior of v_z as well as $|m_c \bar{v}_z|_{ext}$.

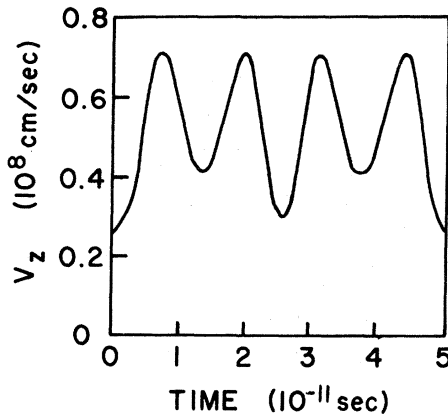FIG. 22. The z component of velocity of an electron at $a\,|\,k_z\,| = 2.6$ versus time for $\vec{B}_0 \parallel [101]$ and $B_0 = 10$ kG.

C. Results and Interpretation for $\vec{B}_0 \parallel [111]$

In Fig. 23, we show the transmitted signal versus B_0 for $\vec{B}_0 \parallel [111]$, and in Fig. 24 we show the differentiated transmitted signal versus B_0 for the same geometry. For this case the GK oscillations appear superimposed on the helicon oscillations. The number of helicon oscillations is limited because the number of effective electrons with $\vec{B}_0 \parallel [111]$ is only about 16% of the number with $\vec{B}_0 \parallel [001]$. It therefore requires a much larger change in B_0 to cause a change in the number of helicon half-wavelengths in the specimen. We will limit ourselves to the information which can be obtained from the GK oscillations.

The period of the GK oscillations shown in Fig. 24 is 590 ± 7 G and shows little variation from the low fields to the high fields. Using this period of 590 ± 7 G a value of $|\,m_c \bar{v}_z\,|_{ext} = (1.26 \pm 0.02) \times 10^{-19}$ g cm sec^{-1} is assigned to those electrons responsible for the GK mode. The corresponding value of $|\,\partial A/\partial k_z\,|_{ext}$ is $(7.50 \pm 0.11) \times 10^8$ cm^{-1}. In Fig. 25 we show a plot of $|\,\partial A/\partial k_z\,|$ versus $a\,|\,k_z\,|$. The horizontal line represents the experimental result. The calculated value of $|\,\partial A/\partial k_z\,|_{ext}$ is 8.05×10^8 cm^{-1}.

V. SUMMARY

GK oscillations and DSCR of helicons have been investigated in very pure copper. The periods of the GK oscillations for $\vec{B}_0 \parallel [101]$ and for $\vec{B}_0 \parallel [111]$ have been found to be a good measure of $|m_c \bar{v}_z|_{ext}$ for these geometries. No GK oscillations were observed with $\vec{B}_0 \parallel [001]$. An explanation is proposed for their absence.
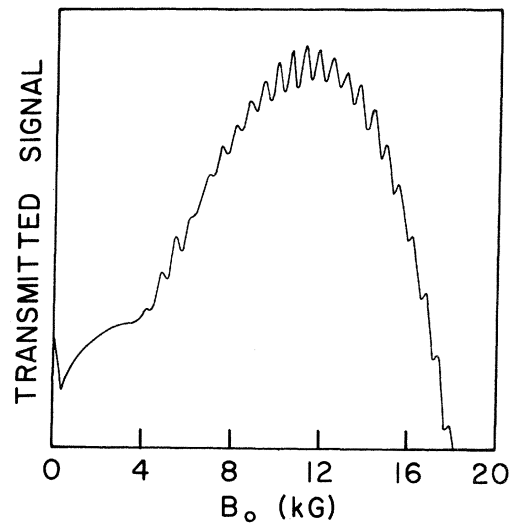

FIG. 23. Transmitted signal versus B_0 for $\vec{B}_0 \parallel [111]$ with $f = 25.0$ kHz, specimen thickness $= 0.84$ mm, and $T = 4.2\,°$K.
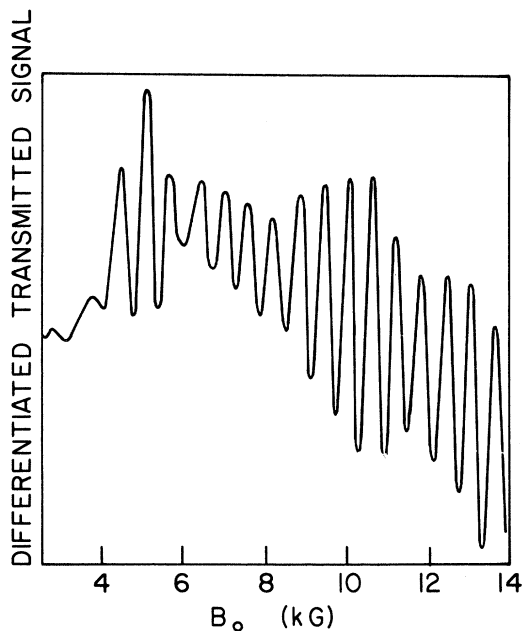
FIG. 24. Differentiated transmitted signal versus B_0 for $\vec{B}_0 \parallel [111]$ with $f = 25.0$ kHz, specimen thickness $= 0.84$ mm, and $T = 4.2$ °K.

FIG. 25. $|\partial A/\partial k_z|$ versus $a|k_z|$ for copper Fermi surface with k_z along [111]. The dashed line indicates where $\partial A/\partial k_z$ is positive, the solid where it is negative. The horizontal line represents the experimental value of $|\partial A/\partial k_z|_{ext}$.

For $\vec{B}_0 \parallel [101]$ a mechanism for exciting the GK mode is proposed. Damping of the helicon by open-orbit electrons has also been observed for this geometry. For $\vec{B}_0 \parallel [001]$ the helicon edge does not seem to be a measure of $|\partial A/\partial k_z|_{max}$.

Finally, we have shown that the information obtained from helicon experiments is consistent with results obtained from magnetoresistance measurements. We have also pointed out the consequences of failure to align the magnetic field along a crystal axis.
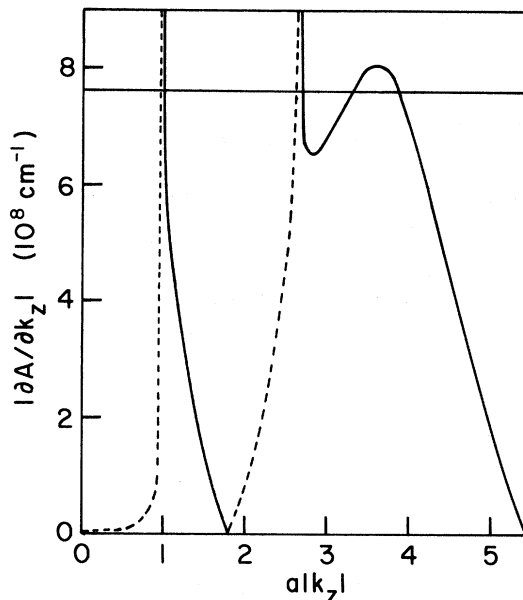
ACKNOWLEDGMENTS

†Work supported by a grant from the National Science Foundation.

*Based in part on a Ph. D. dissertation by L. T. Wood, University of Texas, 1968 (unpublished).

‡ Present address: Department of Physics, University of Houston, Houston, Tex. 77004.

[1]P. Aigrain, in *Proceedings of the International Conference on Semiconductor Physics, Prague, 1960* (Czechoslovak Academy of Science, Prague, 1961), p. 224.

[2]O. V. Konstantinov and V. I. Perel, Zh. Eksperim. i Teor. Fiz. 38, 161 (1960) [Soviet Phys. JETP 11, 117 (1960)].

[3]R. Bowers, C. Legendy, and F. E. Rose, Phys. Rev. Letters 7, 339 (1961).

[4]F. E. Rose, M. T. Taylor, and R. Bowers, Phys. Rev. 127, 1122 (1961).

[5]R. G. Chambers and B. K. Jones, Proc. Roy. Soc.

(London) A270, 417 (1962).

[6]M. T. Taylor, J. R. Merrill, and R. Bowers, Phys. Rev. 129, 2525 (1963).

[7]P. Cotti, P. Wyder, and A. Quattropani, Phys. Letters 1, 50 (1962).

[8]E. A. Stern, Phys. Rev. Letters 10, 91 (1963).

[9]T. Kjeldaas, Phys. Rev. 113, 1473 (1959).

[10]M. T. Taylor, Phys. Rev. 137, A1145 (1965).

[11]J. L. Stanford and E. A. Stern, Phys. Rev. 144, 534 (1966).

[12]V. F. Gantmakher and E. A. Kaner, Zh. Eksperim. i Teor. Fiz. 48, 1572 (1965) [Soviet Phys. JETP 21, 1053 (1965)].

[13]A. W. Overhauser and S. Rodriguez, Phys. Rev. 141, 431 (1966).

[14]J. C. McGroddy, J. L. Stanford, and E. A. Stern, Phys. Rev. 141, 437 (1966).

[15]P. M. Platzman and S. J. Buchsbaum, Phys. Rev.

132, 2 (1963).
[16]G. L. Flint, Jr., M. A. thesis, University of Texas, 1968 (unpublished).
[17]G. A. Baraff, Phys. Rev. 178, 1155 (1969).
[18]P. R. Antoniewicz (unpublished).
[19]C. C. Grimes and S. J. Buchsbaum, Phys. Rev. Letters 12, 357 (1964).
[20]Obtained from A. F. Clark, National Bureau of Standards, Boulder, Colo.
[21]P. R. Antoniewicz, Phys. Letters 24A, 83 (1967).
[22]S. G. Eckstein, Phys. Rev. Letters 16, 611 (1966).
[23]P. R. Antoniewicz, L. T. Wood, and J. D. Gavenda,

Phys. Rev. Letters 21, 998 (1968).
[24]W. A. Harrison, Phys. Rev. 118, 1190 (1960).
[25]M. R. Halse, Phil. Trans. Roy. Soc. London A265, 507 (1969).
[26]S. J. Buchsbaum and P. A. Wolff, Phys. Rev. Letters 15, 406 (1965).
[27]C. C. Grimes, G. Adams, and P. H. Schmidt, Phys. Rev. Letters 15, 409 (1965).
[28]P. R. Antoniewicz (unpublished).
[29]J. R. Klauder, W. A. Reed, G. F. Brennert, and J. E. Kunzler, Phys. Rev. 141, 592 (1966).

Proposed $X_{\alpha\beta}$ Method for Solids*

A. M. Boring

University of California, Los Alamos Scientific Laboratory, Los Alamos, New Mexico 87544

(Received 30 March 1970)

Results of atomic calculations pertinent to the use of Herman's $X_{\alpha\beta}$ method in energy-band calculations are given. With α fixed at $\frac{2}{3}$, two β parameters were determined for each atom, one satisfying the virial theorem, and the other the variational principle. The object of these calculations was to determine the sensitivity of β to changes in charge-density inhomogeneity in going from one atom to the next and the sensitivity to the potential shift of a given atom obtained by turning on the Latter potential. These results are compared with those of Kmetko on the X_{α} method. The results reported here indicate that a β of 0.0040 should be used in applying the $X_{\alpha\beta}$ method in solids.

In this paper the results of a study of the sensitivity of Herman's $X_{\alpha\beta}$ local-exchange potential[1] to the Latter potential and the inhomogeneous charge density in atomic systems are reported. Slater has suggested[2] a method, based on the determination of the α parameter in the free atom, for using the X_{α} local-exchange potential in a crystal. In a crystal one can only determine the energy by the statistical method, so the variational principle and the virial theorem are not available to aid in the determination of α. For this reason Slater has proposed that one use X_{α} orbitals for the atom and determine both the α that satisfies the virial theorem and the different α that minimizes the total energy of the atom as calculated via Hartree-Fock theory. Slater has indicated that the α that satisfies the virial theorem would be the more appropriate one to use in the crystal.

Kmetko[3] has obtained the set of α's that minimize the total energy for all atoms in the Periodic Table. He obtained results both with and without the Latter potential. Since Kohn and Sham[4] have shown that for a nearly homogeneous electron gas the variational principle requires $\alpha = \frac{2}{3}$ for the one-electron eigenvalue equations, deviations from this value can be taken as an indication of the inhomo-

geneity of the system.

In Herman's $X_{\alpha\beta}$ method this inhomogeneity is accounted for by including gradient corrections in the local exchange. The local-exchange operator is then written as

$$V_{X}^{\alpha\beta}(r) = [\alpha + \beta G(r)] V_{XS}(r), \tag{1}$$

where

$$G(r) = \frac{1}{\rho^{2/3}(r)} \left[\frac{4}{3} \left(\frac{\nabla\rho(r)}{\rho(r)} \right)^2 - 2 \frac{\nabla^2\rho(r)}{\rho(r)} \right]$$

and

$$V_{XS}(r) = -6 \left(\frac{3\pi}{8} \rho(r) \right)^{1/3},$$

and $\rho(r)$ is the self-consistent charge density.

Herman has shown the oscillating structure of $G(r)$ for the krypton atom,[5] and this structure was found to be typical of all the atoms studied.

Since the main goal of this study was to determine the sensitivity of β, α was set to the homogeneous-electron-gas value of $\frac{2}{3}$. The β that satisfied the virial theorem (β_v) and the β that minimized the total energy (β_{min}) when calculated via Hartree-Fock theory were then determined. In order to make a general study, but without studying